Plasmon-polariton fractal spectra in quasiperiodic multilayers

M. S. Vasconcelos and E. L. Albuquerque
Departamento de Física, Universidade Federal do Rio Grande do Norte, 59.072-970 Natal-RN, Brazil
(Received 16 May 1997; revised manuscript received 12 August 1997)

We carry out a theoretical analysis for the spectra of plasmon polaritons in multiple semiconductor layers arranged in a quasiperiodical fashion. This quasiperiodicity can be of the type of so-called substitutional sequences. They are characterized by the nature of their Fourier spectrum, which can be dense pure point (Fibonacci sequences) or singular continuous (Thue-Morse and double-period sequences). These substitutional sequences are described in terms of a series of generations that obey peculiar recursion relations. In order to study the plasmon-polariton spectra, we use a convenient theoretical model based on a transfer-matrix treatment, with the layers characterized by a frequency-dependent dielectric function, including the effect of retardation. We present numerical results to discuss the fractal aspect of the spectra, and compare it with the nonfractal spectra presented in the periodic case.
[S0163-1829(98)02905-1]

I. INTRODUCTION

The pioneering experimental works of Merlin and collaborators[1] on nonperiodic Fibonacci and Thue-Morse GaAs-AlAs superlattices have generated a large amount of research activity in the field of quasicrystals. These quasicrystals are formed by the superposition of two (or more) incommensurate periods, so that they can be defined as intermediate systems between a periodic crystal and the random amorphous solids.[2] One of the main motivations to study these structures is because it was recognized that localization of electronic states, one of the most active fields in condensed matter physics,[3] could occur not only in disordered systems, but also in the deterministic quasiperiodic systems.[4]

Localization due to the electronic properties of a tight-binding Schrödinger equation was studied in one dimension by several groups.[5–8] On the other hand, polariton spectra were also reported by Albuquerque and collaborators,[9–12] and they could provide an excellent way to probe experimentally these localized states. The reason for that is because the localization phenomenon is essentially due to the wave nature of the electronic states, and thus could be found in any wave phenomena. Furthermore, there are distinct advantages to studying localization using a classical wave equation instead of the quantum mechanical electronic problem. Indeed, the latter usually deals with other types of interactions, such as, to name a few, spin-orbit effects and the electron-electron interaction.

In disordered dielectric materials, experimental proof of the complete localization of light waves is a difficult task. Complete localization would be indicated by a vanishing diffusion coefficient. Recently, an unusually small optical diffusion coefficient consistent with the onset of localization has been realized in transmission and scattering experiments with microwaves in a random mixture of aluminum and Teflon spheres,[13] where theoretically predicted scaling properties of the transmission with sample thickness were verified. Also, very recently,[14] the optical transmission of quasiperiodic dielectric multilayer stacks of SiO_2 and TiO_2 thin film, ordered according to a Fibonacci sequence, was measured, and the spectrum was in good agreement with the theoretical predictions.

A rather fascinating feature of these quasiperiodic structures is that they exhibit collective properties not shared by their constituents. Therefore, the long-range correlations induced by the construction of these systems are expected to be reflected someway in their various spectra (light propagation, electronic transmission, density of states, polaritons, etc.), defining a novel description of disorder.[15–17] Indeed, theoretical transfer-matrix treatments[18–20] show that these spectra are fractals. On the other hand, the procedure to grow these kind of structures became standard since the pioneering works of Merlin *et al.*[1] It involves defining two distinct building blocks, each of them carrying out the necessary physical information, and having them ordered in a desired manner (for instance, they can be described in terms of a series of generations that obey a particular recursion relation). The presence of long-range correlations in this and other systems avoids canonical approaches like perturbation theory, where one first separates a small localized piece of the system, treating the rest as a perturbation *a posteriori*. This approach does not work in those cases, because the behavior of the macroscopic system is completely distinct from the behavior of its separated small piece, due to the long-range correlations. Fortunately, the presence of long-range correlations itself gives the key to overcome this difficulty: Normally these systems are very robust, to wide modifications on a microscopic scale.

In the study of continuous phase transitions, for instance, the critical behavior is known to depend only upon global properties, namely, the geometric dimension of the system and the symmetries of its order parameter. It is insensitive to the details of the microscopic interactions between atoms or molecules, and then one can classify the various systems in a few *universality classes*.

The aim of this work is twofold: First we want to show the plasmon-polariton spectra of multiple semiconductor layers in quasiperiodic arrangements. These spectra generalize previous investigation in the field (for a review see Refs. 21

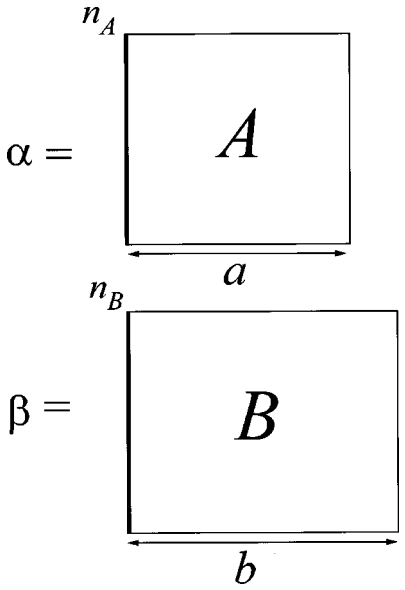

FIG. 1. Schematic representation of the building blocks for the quasiperiodic structures.

and 22). Then, we intend to present a quantitative analysis of the results, pointing out the distribution of the polariton bandwidths for high generations, which gives a good insight about their localization and their power laws, which are a guide to their *universality classes*.

The plan of this work is as follows: In Sec. II, we present the method of calculation employed here, which is based on the transfer-matrix approach. The plasmon-polariton dispersion relation is then determined, and its expression follows the pattern already shown in previous work.[22] Section III is devoted to a discussion of this dispersion relation for various quasiperiodic structures. In Sec. IV we show the numerical results of these spectra, with a discussion of their main features. The conclusions of this work are presented in Sec. V.

II. GENERAL THEORY

In this section we present the general model to describe the polariton dispersion relation in a periodic superlattice. The extension to more complex structures will be given in the next section.

To set up a periodic semiconductor superlattice, we consider two different building blocks (see Fig. 1) which are arranged in the alternated way $\alpha\beta\alpha\beta\cdots$. The building block $\alpha(\beta)$ consists of a two-dimensional electron gas (2DEG) with a carrier concentration $n_A(n_B)$ supported by a dielectric layer $A(B)$. The layers A and B are characterized by the dielectric functions $\epsilon_A(\omega)$ and $\epsilon_B(\omega)$, and have thicknesses a and b, respectively.

In order to find the bulk polariton modes, we consider an infinite structure, where the Cartesian axes are chosen in such a way that the z axis is normal to the xy plane of the layers. Let us assume that the propagation of the electromagnetic wave is p polarized. The 2DEG at each interface is modeled due to the presence of a surface density of current whose expression, given by Ohm's law, is

$$J_{x\xi}=i\omega\epsilon_0\sigma_\xi E_{x\xi}, \tag{1}$$

where

$$\sigma_\xi=\frac{n_\xi e^2}{m^*\omega(\omega+i\gamma_\xi)}. \tag{2}$$

Here, $\xi=A$ or B, n_ξ is the carrier concentration, $e(m^*)$ is the electron's charge (effective mass), ϵ_0 is the vacuum permissivity, and γ_ξ is the damping factor of the material.

To find the polariton bulk dispersion relation, one should solve the electromagnetic wave equation within the layers A and B of the nth unit cell of the superlattice. Then, taking into account Maxwell's boundary conditions, we can find the appropriate (unimodular) transfer matrix for the periodic superlattice, which is expressed by[22]

$$T=N_A^{-1}M_AN_B^{-1}M_B. \tag{3}$$

Here the forms of the matrices M_ξ and N_ξ ($\xi=A$ or B) can be found in Ref. 20.

Now using Bloch's ansatz, we obtain the dispersion relation for the bulk polariton modes, i.e.,

$$\cos(QL)=(1/2)\mathrm{Tr}(T), \tag{4}$$

where Q is the Bloch wave vector and L is the thickness of the unit cell ($L=a+b$).

On the other hand, to set up the dispersion relation of the surface polariton modes, we consider that the infinite superlattice is truncated at $z=0$, and that the region $z<0$ is filled by a transparent medium C, whose frequency-independent dielectric constant is ϵ_C. This semi-infinite superlattice does not possess full translational symmetry in the z direction through multiples of the size of the unit cell L, and therefore we may no longer assume Bloch's ansatz as in the bulk case. However, Eq. (4) still holds provided we replace Q by $i\beta$, i.e.,

$$\cosh(\beta L)=(1/2)\mathrm{Tr}(T). \tag{5}$$

Since we now have to consider the boundary conditions at the new interface at the plane $z=0$, this imposes a further constraint in Eq. (5) which enables us eventually to determine the attenuation factor β. This is given by[22]

$$T_{11}+T_{12}\lambda=T_{22}+T_{21}\lambda^{-1}, \tag{6}$$

with

$$\lambda=(\epsilon_A'+\epsilon_C')/(\epsilon_A'-\epsilon_C'), \tag{7}$$

$$\epsilon_\xi'=\epsilon_\xi(\omega)/\alpha_\xi, \tag{8}$$

and

$$\alpha_\xi=\begin{cases}[k_x^2-\epsilon_\xi(\omega/c)^2]^{1/2} & \text{if } k_x>\epsilon_\xi^{1/2}(\omega/c),\\ i[\epsilon_\xi(\omega/c)^2-k_x^2]^{1/2} & \text{if } k_x<\epsilon_\xi^{1/2}(\omega/c).\end{cases} \tag{9}$$

Here T_{ij} $(i,j=1,2)$ are elements of the transfer matrix T and ϵ_ξ is the dielectric function of the medium in consideration (A or B); k_x is the common in-plane wave vector, ω is the angular frequency, and c is the velocity of the light in vacuum.

Equation (6) represents an implicit dispersion relation for the surface polariton modes. Once it is solved, we can obtain

a value for β which must satisfy Eq. (5) with the requirement $\mathrm{Re}(\beta)>0$ to ensure the localization.

This method can now be extended for more complex superlattices, where it should be necessary to calculate other transfer matrices T for the structure in consideration. Then one should use Eqs. (4), (5), and (6), to find the bulk and surface polariton modes.

III. TRANSFER-MATRIX APPROACH

We now intend to investigate the bulk and surface plasmon-polariton modes in structures that exhibit deterministic disorders, i.e., Fibonacci, Thue-Morse, double-period, and Cantor superlattices, by using the calculations of the previous section.

A Fibonacci structure can be grown experimentally by juxtaposing the two building blocks α and β in such a way that the nth stage of the superlattice S_n is given iteractively by the rule $S_n=S_{n-1}S_{n-2}$, for $n\geqslant 2$, with $S_0=\beta$ and $S_1=\alpha$. It is also invariant under the transformations $\alpha\rightarrow\alpha\beta$ and $\beta\rightarrow\alpha$. The Fibonacci generations are

$$S_0=[\beta],\quad S_1=[\alpha],\quad S_2=[\alpha\beta],\quad S_3=[\alpha\beta\alpha],\ \text{etc.} \tag{10}$$

The number of the bulding blocks increases according to the Fibonacci number, $F_l=F_{l-1}+F_{l-2}$ (with $F_0=F_1=1$), and the ratio between the number of building blocks α and the number of building blocks β in the sequence is equal to the golden mean number $\tau=\frac{1}{2}(1+\sqrt{5})$. The transfer matrices for the Fibonacci generations are as follows.

(a) For $S_0=[\beta]$ or $S_1=[\alpha]$,

$$T_{S_0}=N_B^{-1}M_B,\quad T_{S_1}=N_A^{-1}M_A. \tag{11}$$

(b) For $S_2=[\alpha\beta]$,

$$T_{S_2}=N_A^{-1}M_BN_B^{-1}M_A. \tag{12}$$

(c) For any higher generation ($k\geqslant 1$),

$$T_{S_{k+2}}=T_{S_k}T_{S_{k+1}}. \tag{13}$$

Therefore, from the knowledge of the transfer matrices T_{S_0}, T_{S_1}, and T_{S_2} we can determine the transfer matrix of any generation.

The Thue-Morse sequence is defined by $S_n=S_{n-1}S_{n-1}^{+}(n\geqslant 1), S_n^{+}=S_{n-1}^{+}S_{n-1}$, with $S_0=\alpha$ and $S_0^{+}=\beta$. Another way to build up this sequence is through the inflation rules $\alpha\rightarrow\alpha\beta,\beta\rightarrow\beta\alpha$. The number of building blocks in this quasiperiodic system increases with 2^n, while the ratio of the number of the building blocks α to the number of the building block β is constant and equal to unity. The Thue-Morse generations are

$$S_0=[\alpha],\quad S_1=[\alpha\beta],\quad S_2=[\alpha\beta\beta\alpha],\ \text{etc.}, \tag{14}$$

and the transfer matrices for each generation are as follows.

(a) For $S_1=[\alpha\beta]$,

$$T_{S_1}=N_A^{-1}M_BN_B^{-1}M_A=N_A^{-1}T_{\beta_1}T_{\alpha_1}N_A, \tag{15}$$

where

$$T_{\xi_1}=M_j^{-1}N_j(\xi=\alpha,j=A\quad\text{or}\quad\xi=\beta,j=B). \tag{16}$$

(b) For $S_2=[\alpha\beta\beta\alpha]$,

$$T_{S_2}=N_A^{-1}T_{\alpha_1}T_{\beta_1}T_{\beta_1}T_{\alpha_1}N_A=N_A^{-1}T_{\beta_2}T_{\alpha_2}N_A, \tag{17}$$

where

$$T_{\alpha_2}=T_{\beta_1}T_{\alpha_1}, \tag{18}$$

$$T_{\beta_2}=T_{\alpha_1}T_{\beta_1}. \tag{19}$$

(c) For any generation k ($k\geqslant 1$),

$$T_{S_k}=N_A^{-1}T_{\beta_k}T_{\alpha_k}N_A, \tag{20}$$

with

$$T_{\alpha_{k+1}}=T_{\beta_k}T_{\alpha_k}, \tag{21}$$

$$T_{\beta_{k+1}}=T_{\alpha_k}T_{\beta_k}. \tag{22}$$

A similar rule holds for the double-period sequence, where the nth stage is given by $S_n=S_{n-1}S_{n-1}^{+}$, with $S_n^{+}=S_{n-1}S_{n-1}$, $n\geqslant 1$. It is also invariant under the transformations $\alpha\rightarrow\alpha\beta$, $\beta\rightarrow\alpha\alpha$.

The double-period generations are

$$S_0=[\alpha],\quad S_1=[\alpha\beta],\quad S_2=[\alpha\beta\alpha\alpha],\ \text{etc.} \tag{23}$$

The number of bulding blocks for this sequence increases as in the Thue-Morse sequence, i.e., 2^n, but the ratio between the number of the building blocks α to the number of the

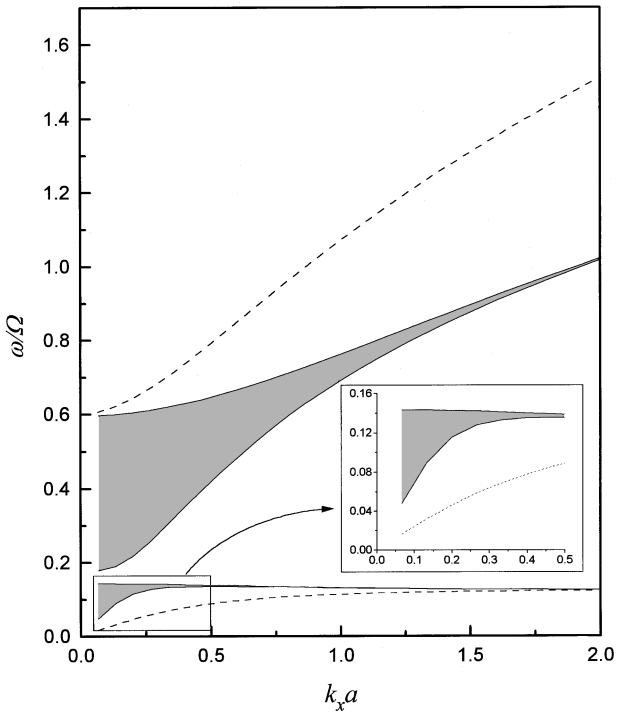

FIG. 2. Plasmon-polariton spectra for the reduced frequency ω/Ω vs k_xa for a periodic superlattice. The physical parameters are given in the main text. The shadow areas represent the bulk bands, while the surface modes are represented by the dashed lines.

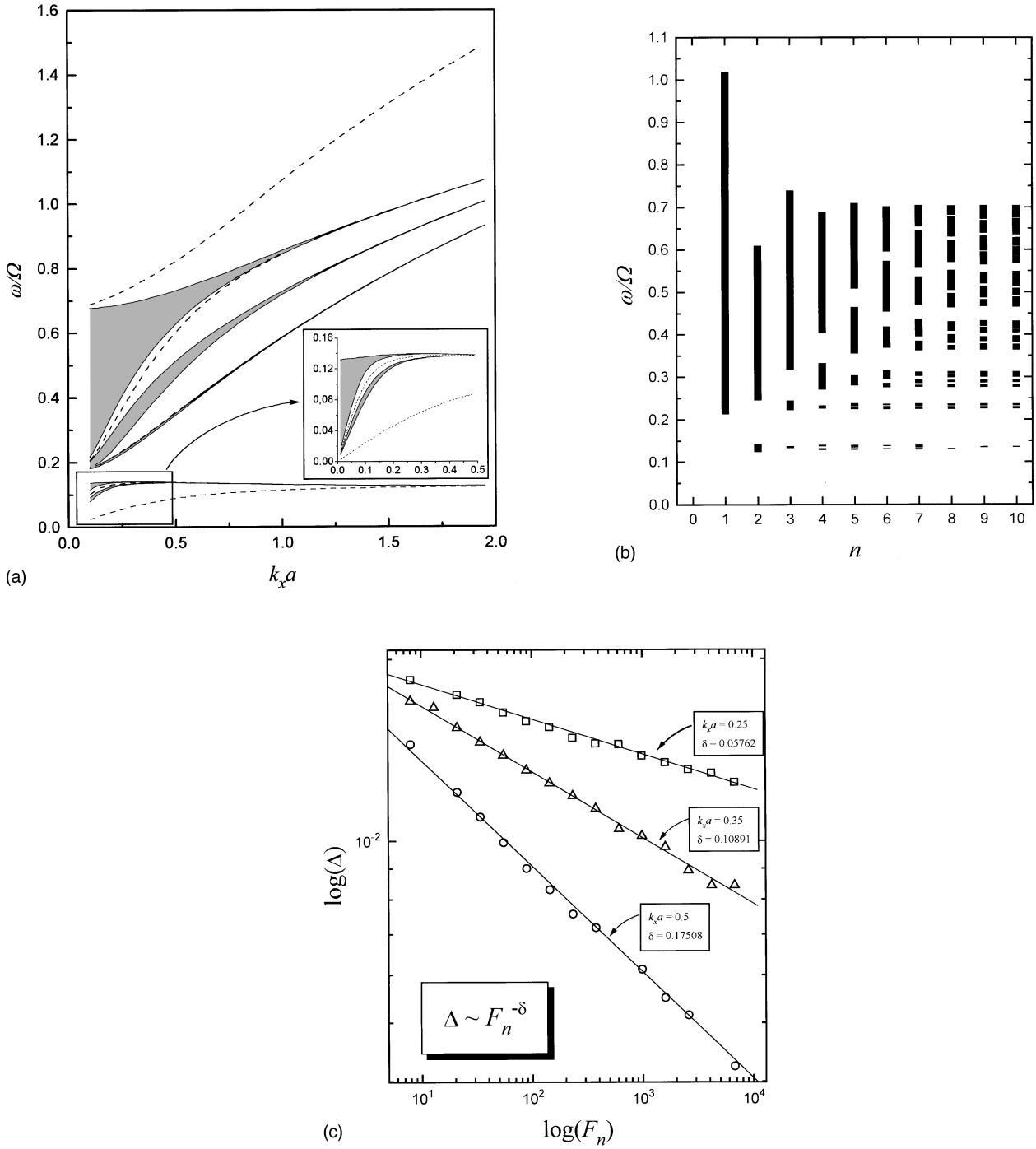

FIG. 3. (a) Same as Fig. 2, but for the quasiperiodic, fourth sequence, Fibonacci superlattice. (b) The distribution of bandwidths for the plasmon polaritons as a function of the Fibonacci generation number n. (c) Log-log plot of the total width of the allowed regions Δ against the Fibonacci number.

building blocks β is not constant; it tends to 2 when the number of generations goes to infinity.

The transfer matrix for the second generation $S_2 = [\alpha\beta\alpha\alpha]$ is given by

$$T_{S_2} = N_A^{-1} M_A N_A^{-1} M_A N_A^{-1} M_B N_B^{-1} M_A \tag{24}$$

or

$$T_{S_2} = T_{S_0} T_{S_0} T_{S_1}. \tag{25}$$

For any generation $k \geq 1$,

$$T_{S_{k+2}} = T_{S_k} T_{S_k} T_{S_{k+1}}. \tag{26}$$

For completeness, we want to investigate also the so-called Cantor superlattice, where the nth stage is given by $S_n = S_{n-1} B_n S_{n-1}$. Here, the nth layer B_n differs from the first layer B_1 only by its thickness $d_{B_n} = 3^{n-1} d_{B_1}$.[11] We can also construct the sequence by the transformations $\alpha \rightarrow \alpha\beta\alpha$, $\beta \rightarrow \beta\beta\beta$. The Cantor generations are

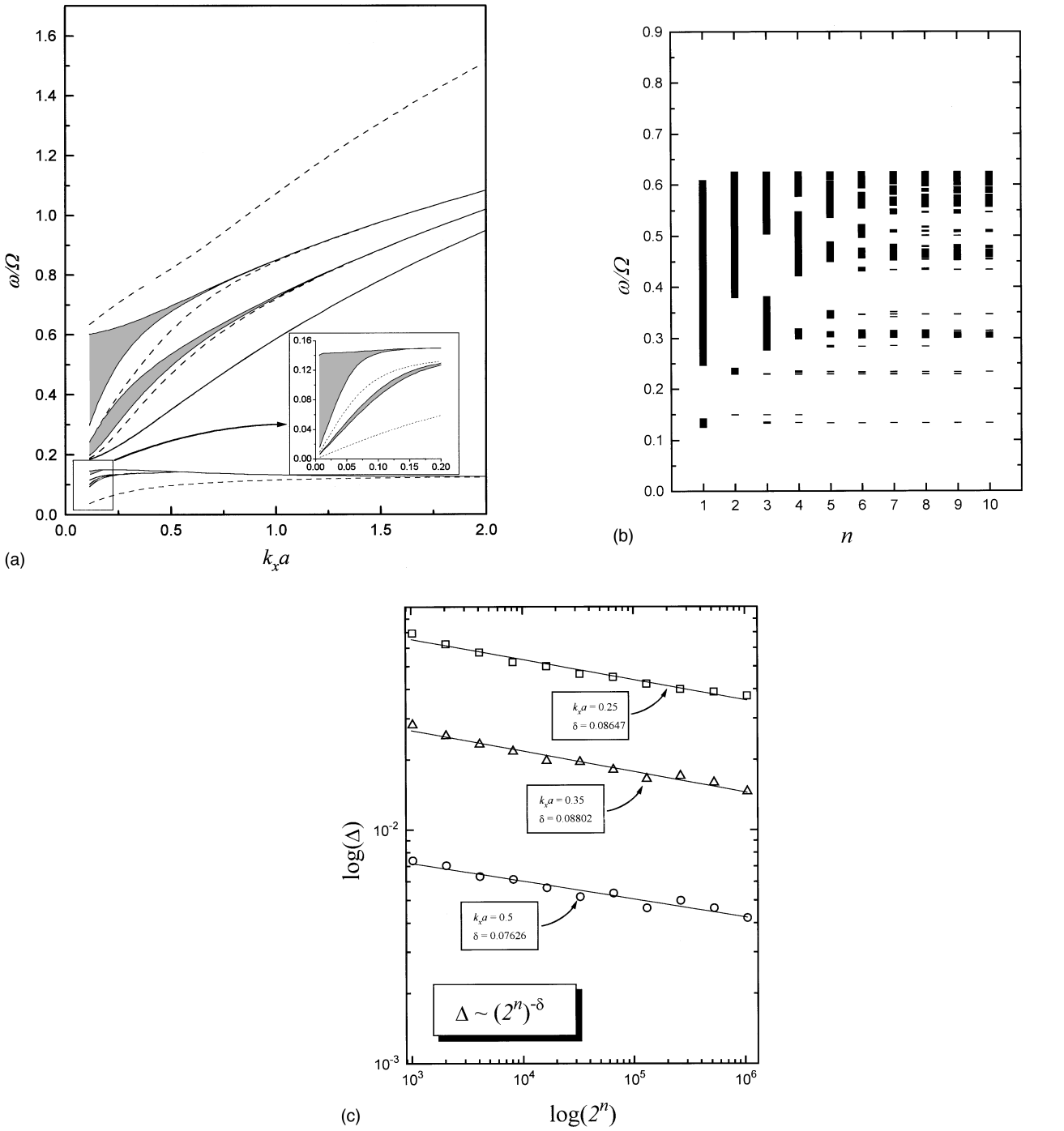

FIG. 4. (a) Same as Fig. 2, but for the quasiperiodic, third sequence, Thue-Morse superlattice. (b) The distribution of bandwidths for the plasmon polaritons as a function of the Thue-Morse generation number n. (c) Log-log plot of the total width of the allowed regions Δ against 2^n.

$$S_0=[\alpha],\quad S_1=[\alpha\beta\alpha],\quad S_2=[\alpha\beta\alpha\beta\beta\beta\alpha\beta\alpha],\ \text{etc.} \tag{27}$$

The transfer matrix for the nth generation of this sequence is

$$T_{S_n}=T_A T_n, \tag{28}$$

where

$$T_A=N_A^{-1}M_A \tag{29}$$

and

$$T_n=T_{n-1}T_{AB_n}T_{n-1}\quad (n\geq 2), \tag{30}$$

with

$$T_{AB_n}=N_A{}^{-1}M_{B_n}N_{B_n}{}^{-1}M_A \tag{31}$$

and

$$T_1=T_{AB_1}. \tag{32}$$

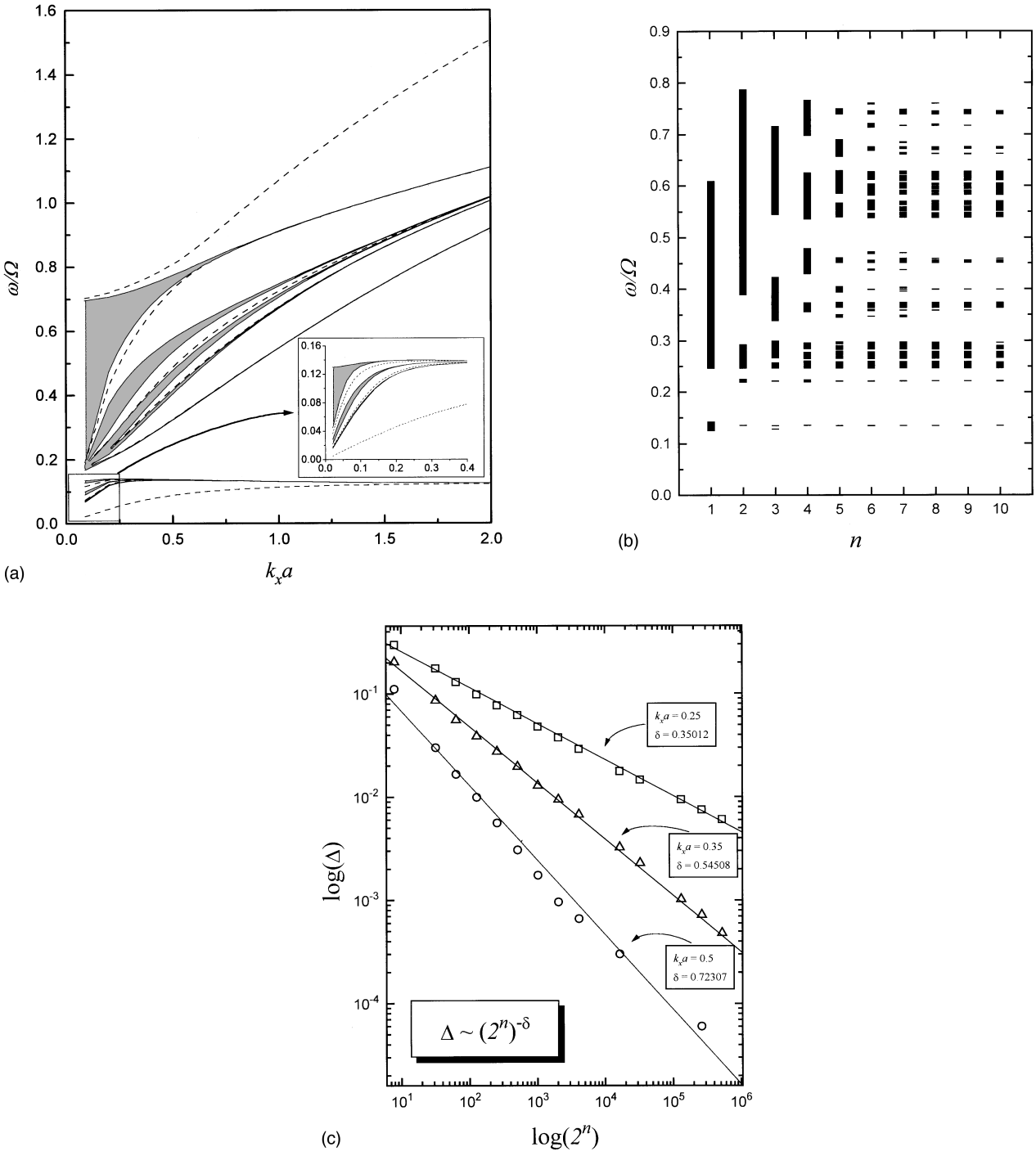

FIG. 5. (a) Same as Fig. 2, but for the quasiperiodic, third sequence, double-period superlattice. (b) The distribution of bandwidths for the plasmon polaritons as a function of the double-period generation number n. (c) Log-log plot of the total width of the allowed regions Δ against 2^n.

With the knowledge of all these transfer matrices, we can now calculate the plasmon-polariton spectra (bulk and surface modes) for these artificial structures, and this is the topic of the next section.

IV. NUMERICAL RESULTS

In this section we present some numerical results to characterize the spectrum of the polariton (bulk and surface modes) that can propagate in the quasiperiodic structures described in the last section. We consider medium A as GaAs, whose frequency-dependent dielectric function, appropriated for the interaction of the electromagnetic radiation with plasmons, is given by

$$\epsilon_A = \epsilon_{\infty A}\left[1 - \frac{\omega_{pA}^2}{\omega(\omega + i\Gamma_A)}\right]. \tag{33}$$

Here, $\epsilon_{\infty A}$ is the background dielectric constant, ω_{pA} is the plasma fequency, and Γ_A is the damping factor. For medium

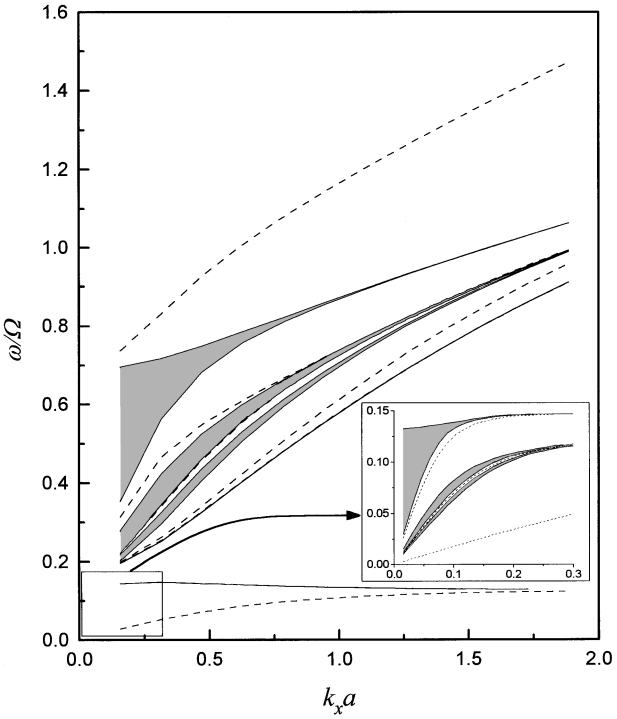

FIG. 6. Same as Fig. 2, but for the quasiperiodic, second sequence, Cantor superlattice.

B, we consider the physical parameters of SiO_2, whose frequency-independent dielectric function is $\epsilon_B = 12.3$. The other physical parameters used here are $\epsilon_{\infty A} = 12.9$, $\epsilon_{\infty B} = \epsilon_B = 12.3$, $n_a = n_b = 6 \times 10^5$ m^{-2}, $m_A^* = 6.4 \times 10^{-32}$ kg, $a = b/2 = 40$ nm, $\omega_{pA} = 4.04$ THz, and $\Gamma_A = \gamma_A = 0$. We also consider medium C to be the vacuum ($\epsilon_C = 1$).

For numerical results, instead of using the frequency ω, we prefer to replace it by the reduced frequency ω/Ω where Ω is given by

$$\Omega = \left(\frac{\epsilon_{\infty A} n_A e^2}{m^* \epsilon_0 a} \right)^{1/2}. \tag{34}$$

For GaAs the value of Ω is approximately equal to 23 THz.

The plasmon-polariton spectra for the periodic, as well as the quasiperiodic Fibonacci, Thue-Morse, double-period, and Cantor superlattices, are presented in Figs. 2, 3(a), 4(a), 5(a), and 6, respectively. In all these spectra the surface modes are represented by the dashed lines, while the bulk bands are characterized by the shadow areas, which are limited by the equations $QL = 0$ and $QL = \pi$. These spectra encompass those found in the literature so far.[22]

For the periodic case, depicted in Fig. 2, the plasmon-polariton spectrum has two well-defined branches. The high-frequency branch is in the range $0.18 < \omega/\Omega < 0.6$, for $k_x \simeq 0$, while the low-frequency one lies in the region $\omega/\Omega < 0.17$ for the same value of k_x. The high-frequency surface mode merges from the bulk band at $\omega/\Omega = 0.6$, and then evolves quite apart from the bulk band. The low-frequency surface mode, on the other hand, starts at $\omega/\Omega = 0$ and then merges into the bulk band at $\omega/\Omega \simeq 0.126$ for $k_x a \simeq 2.6$. The inset in this figure shows clearly that the spectrum has no self-similarity pattern.

In Fig. 3(a) we present the plasmon-polariton spectrum for the fourth Fibonacci generation. Observe that the number of bulk bands is equal to the Fibonacci number F_4, and indeed, in general, this number is always equal to the Fibonacci number of the correspondent generation. There are two surface modes which have a behavior similar to that found in the periodic case: a high-frequency one, which starts at the bulk band and then propagates quite apart of it for high $k_x a$, and a low-frequency mode, which starts away of the bulk band, merging to it at $k_x a \simeq 2.6$. Quite interesting, the later property holds for *all* quasiperiodic structures studied here. The inset of this figure is a qualitative indication of the fractal aspect of the spectrum. The distribution of the bandwidths is shown in Fig. 3(b), for $k_x a = 0.25$. From there, one can infer the forbidden and allowed energies as a function of the generation number n up to the tenth generation of the Fibonacci sequence, which means a unit cell with 55 α and 34 β building blocks. Notice that, as expected, for large n the allowed band regions get narrower and narrower, as an indication of more localized modes. In fact, the total width of the allowed regions in energy goes down as the power law $\Delta \sim F_n^{-\delta}$, where F_n is the Fibonacci number and the exponent δ is a function of the common in-plane wave vector $k_x a$. In Fig. 3(c) we show a log-log plot of these power laws for three different values of $k_x a$, namely, 0.25, 0.35, and 0.5.

The Thue-Morse quasiperiodic third generation is shown in Fig. 4(a). Here, as in the previous cases, we have two well-defined regions for the plasmon-polariton spectrum. The number of bulk bands increases as $2^n + 1$, n being the Thue-Morse generation. The surface modes lie between the bulk bands. The qualitative self-similarity aspect of the spectrum is apparent in the inset. Figure 4(b) shows the forbidden and allowed regions of propagation for the plasmon polaritons as a function of the Thue-Morse generation number. We went up to the tenth generation of the sequence, which means a unit cell with 2^{10} α and β building blocks. The total allowed bandwidth Δ scales as the power law $\Delta \sim (2^n)^{-\delta}$, where now δ is independent of the common wave vector k_x. Indeed, in Fig. 4(c) we can see a log-log plot of the width Δ of the allowed regions against 2^n for three different values of $k_x a$, with almost the same value of δ, the small difference probably due to numerical errors.

For the double-period quasiperiodic structure, the plasmon-polariton spectrum for its third generation is shown in Fig. 5(a). It has a spectrum similar to those observed in the Thue-Morse case. However, there is an important difference here: The number of bulk bands in the high-frequency region of the spectrum for each generation is equal to the number of α building blocks of the correspondent generation, while the number of bulk bands in the low-frequency region is equal to the number of β building blocks of the same generation. Altogether, however, the number of bulk bands increases as 2^n. The forbidden and allowed regions, as a function of its generation number n, are shown in Fig. 5(b). The scaling behavior of the allowed bands width Δ is $\Delta \sim (2^n)^{-\delta}$, where here, as in the Fibonacci case, the exponent δ is a function of the common wave vector $k_x a$, as can be seen in Fig. 5(c).

Finally, for completeness, we show in Fig. 6, the plasmon-polariton spectrum for the Cantor superlattice (second generation). Of course it is not inserted in the substitu-

tional classes defined by the other structures. The number of bulk bands obeys the following sequence of numbers:

$$S_n = \begin{cases} 7n/2 & \text{for } n \text{ even,} \\ (7n-1)/2 & \text{for } n \text{ odd.} \end{cases} \quad (35)$$

It has also a qualitative self-similarity aspect, which is clear from the inset of this figure.

V. CONCLUSIONS

In this work we have presented a general theory for the propagation of plasmon polaritons in quasiperiodic superlattices of substitutional types, whose spectra are illustrated by the Figs. 3, 4, and 5. We have studied some physical properties of these substitutional sequences, mainly those related to their self-similarity behavior, whose fractalitity can be described by the power laws depicted in Figs. 3(c), 4(c), and 5(c), not found in the periodic case. Also, we presented some discussion about localization, as expressed by the distribution of their bandwidths shown in Figs. 3(b), 4(b), and 5(b).

The most important experimental techniques to probe these spectra are the inelastic light scattering of Raman type and ATR (attenuated total reflection). In the case of Raman scattering, one uses a grating spectrometer to detect the scattered light. The typical shift of the frequency of the scattered light is in the range 0.6–500 meV, which makes this technique one of the most appropriate to probe the polariton spectra. On the other hand, the ATR spectroscopy is much easier to set up than the Raman one, but with less precise results. However, this technique was employed with success in a number of experiments (for a review see Ref. 23).

ACKNOWLEDGMENTS

We thank Professor A.M. Mariz and Professor C. Tsallis for discussions and a critical reading of the manuscript, and the Brazilian Research Council CNPq for partial financial support.

[1] R. Merlin, K. Bajema, R. Clarke, F.-Y. Juang, and P.K. Bhattacharya, Phys. Rev. Lett. **55**, 1768 (1985); J. Todd, R. Merlin, R. Clarke, K.M. Mohanty, and J.D. Axe, *ibid.* **57**, 1157 (1986); R. Merlin, K. Bajema, J. Nagle, and K. Ploog, J. Phys. (Paris) Colloq. **48**, C5-503 (1987); Z. Cheng, R. Savit, and R. Merlin, Phys. Rev. B **37**, 4375 (1988).

[2] D. Shechtman, I. Blech, D. Gratias, and J.W. Cahn, Phys. Rev. Lett. **53,** 1951 (1984); P.J. Steinhard and S. Ostlund, *The Physics of Quasicrystals* (World Scientific, Singapore, 1987).

[3] For a review, see P.A. Lee and T.V. Ramakrishnan, Rev. Mod. Phys. **57**, 287 (1985).

[4] For a review, see J.B. Sokoloff, Phys. Rep. **126**, 189 (1985).

[5] S. Ostlund, R. Pandit, D. Rand, H.J. Schellnhuber, and E.D. Siggia, Phys. Rev. Lett. **50**, 1873 (1983).

[6] M. Kohmoto and Y. Oono, Phys. Lett. A **102**, 145 (1984).

[7] J.P. Lu, T. Odagaki, and J.L. Birman, Phys. Rev. B **33**, 4809 (1986).

[8] F. Nori and J.P. Rodriguez, Phys. Rev. B **34**, 2207 (1984).

[9] E.L. Albuquerque and M.G. Cottam, Solid State Commun. **81**, 383 (1992); **83**, 545 (1992); Braz. J. Phys. **24**, 260 (1994).

[10] E.L. Albuquerque, Phys. Lett. A **181**, 409 (1993); Solid State Commun. **91**, 251 (1994); **99**, 311 (1996).

[11] M.S. Vasconcelos and E.L. Albuquerque, Physica B **222**, 113 (1996).

[12] P.M.C. de Oliveira, E.L. Albuquerque, and A.M. Mariz, Physica A **227**, 206 (1996).

[13] A.Z. Genack and N. Garcia, Phys. Rev. Lett. **66**, 2064 (1991).

[14] W. Gellermann, M. Kohmoto, B. Sutherland, and P.C. Taylor, Phys. Rev. Lett. **72**, 633 (1994).

[15] J.M. Luck, Phys. Rev. B **39**, 5834 (1989).

[16] F. Axel and H. Terauchi, Phys. Rev. Lett. **66**, 2223 (1991).

[17] J. Bellisard, A. Borier, and J.-M. Ghez, Commun. Math. Phys. **135**, 379 (1991).

[18] M. Kohmoto and J.R. Banavar, Phys. Rev. B **34**, 563 (1986); M. Kohmoto, B. Sutherland, and K. Iguchi, Phys. Rev. Lett. **58**, 2436 (1987); M. Kohmoto, B. Sutherland, and C. Tang, Phys. Rev. B **35**, 1020 (1987).

[19] M. Kolár and M.K. Ali, Phys. Rev. B **39**, 426 (1989); **41**, 7108 (1990).

[20] M. Kolár and M.K. Ali, and F. Nori, Phys. Rev. B **43**, 1034 (1991).

[21] M.G. Cottam and D.R. Tilley, *Introduction to Surface and Superlattices Excitations* (Cambridge University Press, Cambridge, England, 1989).

[22] E.L. Albuquerque and M.G. Cottam, Phys. Rep. **233**, 67 (1993).

[23] N. Raj and D.R. Tilley, in *The Dielectric Function of Condensed Systems*, edited by L.V. Keldysh, D.A. Kirzhnitz, and A.A. Maradudin (North-Holland, Amsterdam, 1989).